Magnetic and magnetoimpedance properties of rapidly quenched ribbons of modified alloys based on FINEMET

Journal of Physics: Conference Series **1389** (2019) 012123 doi:10.1088/1742-6596/1389/1/012123

Magnetic and magnetoimpedance properties of rapidly quenched ribbons of modified alloys based on FINEMET

E A Stepanova[1], S O Volchkov[1], V A Lukshina[1,2], D M Khudyakova[1], A Larrañaga[3] and D S Neznakhin[1]

[1] Ural Federal University, 620002 Ekaterinburg, Russia
[2] Institute of Metal Physics UB RAS, 620137 Ekaterinburg, Russia
[3] Universidad del Pais Vasco and BCMaterials UPV-EHU, 48940 Leioa, Spain

E-mail: elena.stepanova@urfu.ru

Abstract. Amorphous and nanocrystalline materials are attractive systems for basic research and technological applications. In a view of the energy economy and global warming concepts there is a request to search for soft magnetic materials for sensor applications, which do not request additional heat treatments and can be produced in most simple technological scheme. In this work the structure, static magnetic properties and magnetoimpedance (MI) were studied for FINEMET-type materials both with classic composition and for compositions with 10 % of iron substitution by Co, Ni, or Mn in initial state, i.e. without any additional heat treatmnet. The best MI responses were obtained for Mn-doped rapidly quenched ribbons.

1. Introduction

Nanomaterials are attractive systems for basic research and technological applications. They are represented by thin films and multilayered structures, magnetic nanoparticles and nanowires, rapidly quenched ribbons and wires as well as different kinds of patterned structures and nanocomposites [1-3]. Rapidly quenched amorphous and nanocrystalline ribbons are soft magnetic alloys which are currently used for the manufacture of wound magnetic cores [4-5], for magnetic shielding [6], and as sensors of small magnetic fields, including magnetoimpedance-based (MI) sensors [7-8].

The mechanisms of the effect of heat treatments on the magnetic properties of such alloys are well studied. However, comprehensive studies of quasistatic and high-frequency magnetic properties of doped nanocrystalline alloys are still highly relevant as the number of applications is increasing and applications conditions are changing under the technological request. For example, one of the requested directions is MI-materials with simple fabrication process, which does not include additional heat treatments. The last request is driven by energy economy and global warming concepts. Special interest is also observed in the case of nanocrystalline alloys for applications in the extreme conditions such as unexpected heating or high radiation level, typical for technological disaster. Another interesting direction is the search for MI flat sensitive elements which are cheap and do not require additional heat treatments. As the dopant can change crystalline structure, resistivity and magnetic permeability careful comparison of well known MI materials with their doped analogues is a topic of special interest.

In the present study the structure, magnetic properties and magnetoimpedance effect were comparatively analysed for FINEMET-type materials both without doping and for compositions with 10 % of iron substitution by Co, Ni, or Mn both in initial state.

2. Experimental methods

Rapidly quenched ribbons of classic composition and for compositions with 10 % of iron substitution by Co, Ni, or Mn in as-quenched state:

1. $Fe_{73.5}Si_{13.5}B_9Nb_3Cu_1$ (FM),
2. $Fe_{63.5}Co_{10}Si_{13.5}B_9Nb_3Cu_1$(FM-Co),
3. $Fe_{63.5}Ni_{10}Si_{13.5}B_9Nb_3Cu_1$(FM-Ni),
4. $Fe_{63.5}Mn_{10}Si_{13.5}B_9Nb_3Cu_1$ (FM-Mn).

Amorphous ribbons were fabricated by rapid quenching onto the rotating Cu drum surface. Structure was studied by X-ray diffraction technique (XRD) using a Bruker D8 Advance diffractometer equipped with a Cu tube (radiation wave length, k = 1.5406 Å). The sample was mounted onto a zero background silicon plate embedded in a generic sample holder. The crystal size can be accurately determined based on the peak width of the principal XRD peak using the Scherrer formula [9-10].

Magnetic properties were determined by certified MMKS 100-05 apparatus designed for measurements of static magnetic characteristics of the samples in a frequency (f) range of 0.1 to 100 Hz: magnetization curve, maximum magnetic permeability (μ_{max}), magnetic hysteresis loop, and coercive force (H_c) were determined.

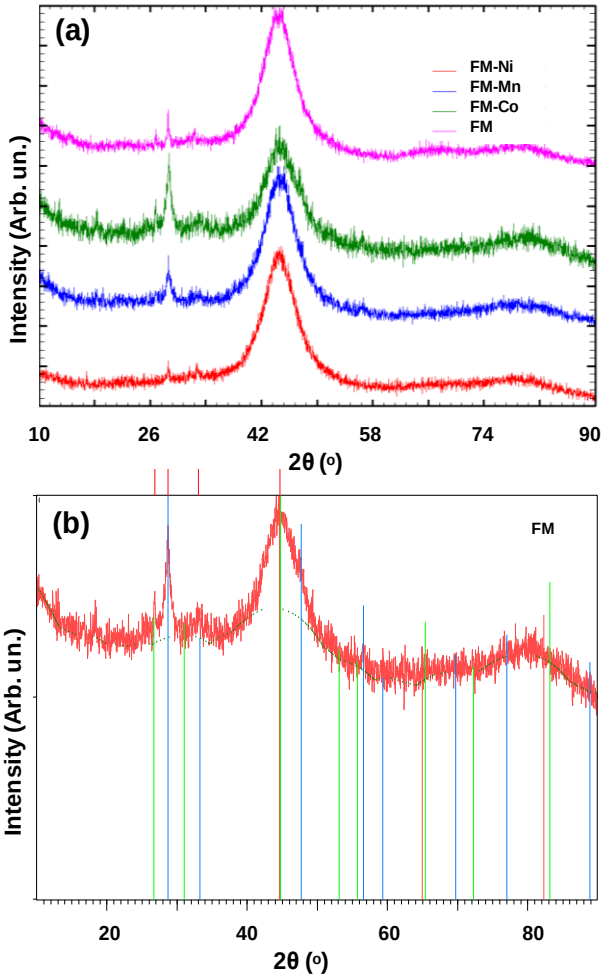

Figure 1. XRD spectra of rapidly quenched ribbons of different compositions (a). Example of phase identification using peak analysis for classic FINEMET ribbon without doping (b).

In order to estimate possible thermal stability and define the Curie temperatures of all materials the temperature dependences of the magnetic moments were measured in the wide temperature range. Complex impedance ($Z= R+iX$, where R is the real and X is the imaginary part of the total impedance) was measured as a function of the magnetic field (H) applied in the direction of the flowing alternating current along the long side of the ribbon. The geometry of the samples for MI measurements was 45 mm × 5 mm and the frequency (f) range of the driving current was 1–400 MHz. Measurements were made in a "microstripe" line using previously described methodology [11-12]. The total impedance and real part values were calculated from the S11 reflection coefficients measured by Agilent E4991A network analyser after calibration and subtraction of the contributions of the test fixtures. The MI ratio defined as follows: for the total impedance: $\Delta Z/Z= 100 \times (Z(H) - Z(H_{max}))/Z(H_{max})$, where $H_{max}= 100$ Oe. The frequency dependence of the maximum MI ratio for total impedance $\Delta Z/Z_{max}$ was also calculated as the maximum value for the $\Delta Z/Z(H)$ dependence obtained at given frequency. The sensitivity of the MI was defined as follows: $S(\Delta Z/Z) = \Delta Z/Z/\Delta H$, where $\Delta H = 0.1$ Oe.

3. Results and discussion

XRD studies confirmed very close to amorphous structure of all samples in the initial state with the grain size about 2 nm or below (figure 1). Preliminary identification of the initial phases was evaluated using the Powder Diffraction File (PDF) database. Although the peaks are very wide, XRD peaks positions were in good agreement with cubic bcc structure for F_3Si phase and fcc structure for Fe phase.

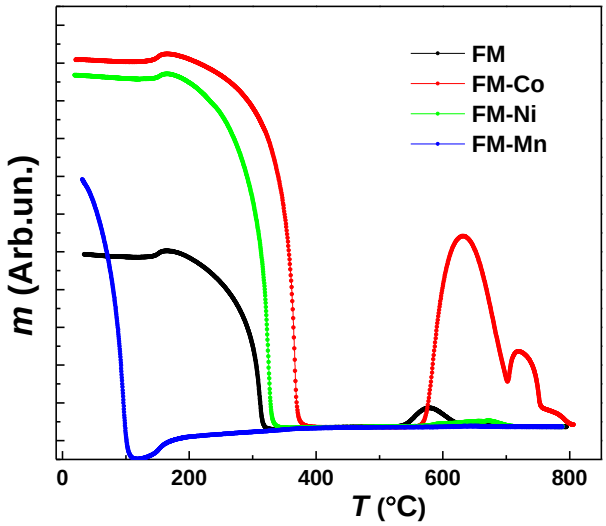

Figure 2. Temperature dependences of the magnetic susceptibility of FINEMET-type ribbons of different compositions without or with doping.

Figure 2 shows the results of the measurements of magnetic susceptibility in the wide temperature range. It was observed that different Curie and crystallization temperatures correspond to different ribbon compositions. The most interesting difference between FM, FM-Co, FM-Ni compositions and FM-Mn case is their rate of the magnetization change in the close to room temperature range.

Magnetic moments (m) of FM, FM-Co and FM-Ni ribbons show almost no variation up to 150 °C but magnetic moment of FM-Mn ribbon shows very fast decay down to almost zero value at the temperature of 100 °C. This means that such a material is very sensitive to the small temperature changes and it might be not appropriate for creation of a magnetic field sensor if the application conditions can include the working temperature variation. At the same time magneto-impedance

sensors were proposed for measurements of the temperature in certain devices [13-14]. Precisely FM-Mn ribbons can be very good candidates for this kind of applications.

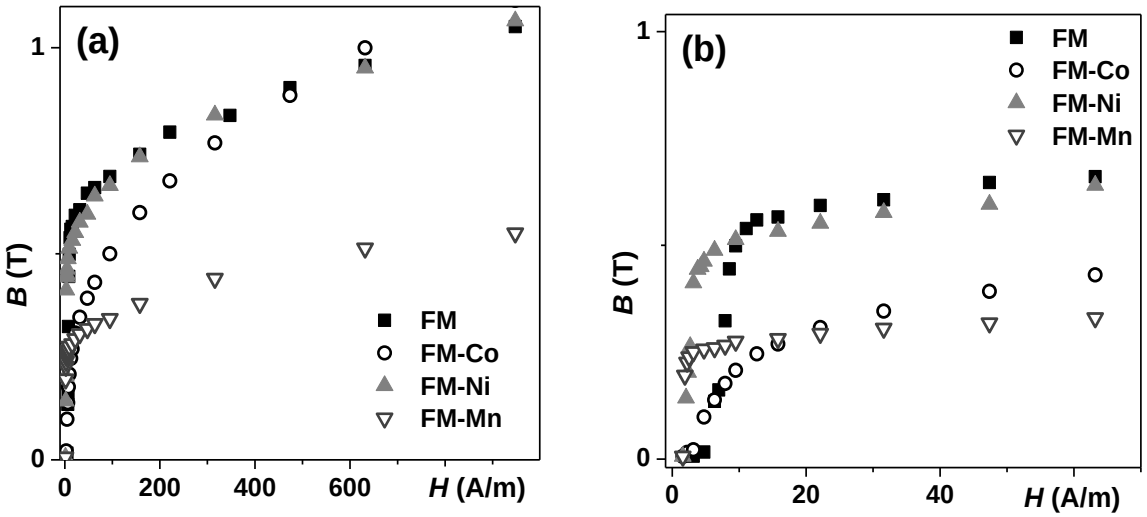

Figure 3. Magnetization curves of $Fe_{73.5}Si_{13.5}B_9Nb_3Cu_1$ (FM)), $Fe_{63.5}Co_{10}Si_{13.5}B_9Nb_3Cu_1$ (FM-Co), $Fe_{63.5}Ni_{10}Si_{13.5}B_9Nb_3Cu_1$ (FM-Ni) and $Fe_{63.5}Mn_{10}Si_{13.5}B_9Nb_3Cu_1$ (FM-Mn) ribbons measured at room temperature: (a) – wide field range, (b) low field range.

Figure 3 shows magnetization curves for amorphous ribbons of all compositions under consideration. One can see that FM, FM-Ni and FM-Co have similar values of saturation magnetization, which is about twice higher of the saturation magnetization obtained in the case of FM-Mn ribbon for the room temperature. FM-Co ribbon has different saturation approach features in comparison with FM and FM-Ni. At the same time low field behaviour, which is most important for MI applications (figure 3(a)) indicates that FM-Co ribbons, despite of low value of saturation magnetization have quite high initial magnetic permeability.

Figure 4(a) shows the field dependences of the total impedance ratio for all ribbons for the frequency of 17 MHz. One can see very clear difference in the total impedance variation. First, as usual, classic FM shows maximum of the $\Delta Z/Z$ of about 10% with clear longitudinal magnetic anisotropy, as to expect for ribbon annealed without magnetic field. FM-Ni ribbon shows lowest impedance variation of a few percent. At the same time, FM-Ni and FM-Mn alloys show maximum of the $\Delta Z/Z$ ratio of about 45 and 60 % accordingly. Although an effective magnetic anisotropy for FM-Ni and FM-Mn ribbons was still longitudinal (one-peak MI response), in a very low field a double peak structure started to appear due to contribution of the surface anisotropy. Such a behaviour was previously discussed in the literature [15].

Figure 4(b) shows the frequency dependence of the maximum of MI ratio in wide frequency range. The difference in the high frequency behaviour become very clear: the highest $\Delta Z/Z_{max}$ ratio value corresponds to the Mn doped ribbon and it is observed for lowest frequency of the driving current of about 20 MHz. Another interesting feature for the $\Delta Z/Z_{max}(f)$ dependences is that above 100 MHz limit the FM-Ni responses become the highest.

In contrast to figure 4a showing $\Delta Z/Z$ data for the frequency below the frequency corresponding to the maximum of $\Delta Z/Z_{max}(f)$ value figure 4(a) shows the field dependences of the total impedance ratio for all ribbons for the frequency of 67 MHz, i.e. for the frequency above the frequency corresponding to the maximum of $\Delta Z/Z_{max}(f)$ value. Here FM-Co and FM-Mn are very close to each other and they have very similar shape that means similar sensitivities with respect to applied magnetic field in all frequency ranges.

Let us now analyse FM-Mn ribbon responses showing the best functional characteristics (figure 5). The best MI responses were obtained for the frequency of 34 MHz: Mn-doped ribbons showed $\Delta Z/Z_{max}$ response of about 64 %. Remarkable change of the shape of the MI curve attract special attention. It transforms from the one-peak type for f = 1-10 MHz to two peaks type for f above 10 MHz range with definite change of the shape the 70 MHz limit, where the transverse anisotropy dominates. Sensor applications request high sensitivities of the sensitive elements in a low magnetic field. Figure 5(b) allows estimate such sensitivities using the $\Delta Z/Z(H)$ curve slope. One can see that the sensitivity of about 3%/Oe was observed in a frequency range of 50 to 150 MHz but the working field interval was different. The highest working field interval (for linear dependence of $\Delta Z/Z(H)$) was observed in the 0.0 to 5.5 Oe range for f = 84 MHz. It corresponds to a work point of about 2.7 Oe being quite good for applications. For comparison, for f = 68 MHz ($0 < H < 4$ Oe) and f = 50 MHz (1.7 Oe $< H <$ 7.0 Oe) the work intervals were narrower and in the last case the work point corresponds to a higher field of about 4.4 Oe.

Observed values of MI ratio and MI ratio sensitivities in the initial state are quite promising as they allow usage of these materials for sensor applications without additional heat treatments.

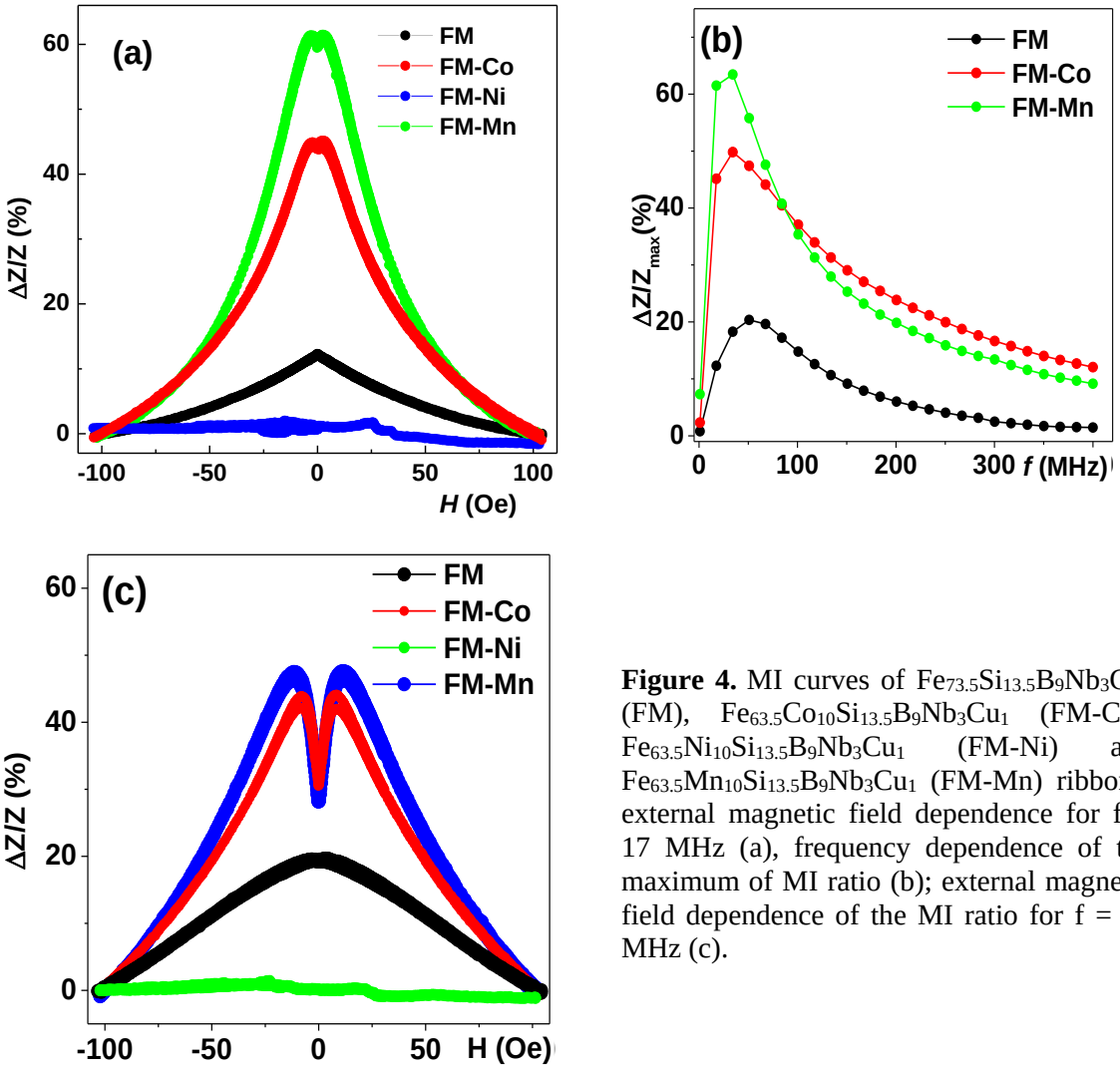

Figure 4. MI curves of $Fe_{73.5}Si_{13.5}B_9Nb_3Cu_1$ (FM), $Fe_{63.5}Co_{10}Si_{13.5}B_9Nb_3Cu_1$ (FM-Co), $Fe_{63.5}Ni_{10}Si_{13.5}B_9Nb_3Cu_1$ (FM-Ni) and $Fe_{63.5}Mn_{10}Si_{13.5}B_9Nb_3Cu_1$ (FM-Mn) ribbons: external magnetic field dependence for f = 17 MHz (a), frequency dependence of the maximum of MI ratio (b); external magnetic field dependence of the MI ratio for f = 68 MHz (c).

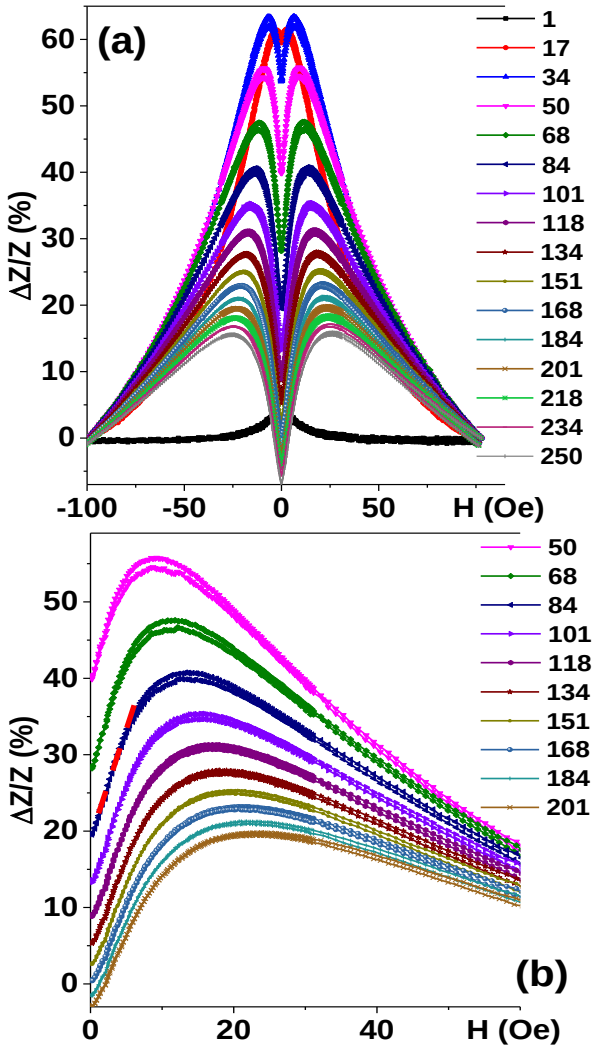

Figure 5. Field dependences of MI ratio for total impedance variation for FM-Mn ribbons: wide frequency and field range (a), narrow frequency and field range (b). Numbers in the legends correspond to the frequencies of the driving current. Red dashed line indicates interval of the highest sensitivity with respect to applied magnetic field.

4. Conclusion

Amorphous ribbons of $Fe_{73.5}Si_{13.5}B_9Nb_3Cu_1$; $Fe_{63.5}Co_{10}Si_{13.5}B_9Nb_3Cu_1$, $Fe_{63.5}Ni_{10}Si_{13.5}B_9Nb_3Cu_1$ and $Fe_{63.5}Mn_{10}Si_{13.5}B_9Nb_3Cu_1$ compositions were prepared by the rapid quenching technique. Their structure, static magnetic properties and magnetoimpedance were comparatively studied in as-quenched state.

The best MI responses were obtained for Mn-doped ribbons showing $\Delta Z/Z_{max}$ response of about 64 % for the frequency of 34 MHz. The sensitivity of about 3%/Oe was observed in a frequency range of 50 to 150 MHz. The highest working field interval (for linear dependence of $\Delta Z/Z(H)$) was in the 0.0 to 5.5 Oe range for f = 84 MHz with a work point for possible sensor device of about 2.7 Oe being quite good for applications.

Acknowledgments
The results were obtained under financial support of the state task of the Ministry of Education and Science of Russia 3.6121.2017/8.9. We thank D. Schishkin for special support.

References

[1] Antonov A S, Gadetskii S N, Granovskii A B, D’yachkov A L, Paramonov V P, Perov N S, Prokoshin A F, Usov N A and Lagar’kov A N 1997 *Phys. Met. Metallogr.* **83** 612
[2] Darton N J, Ionescu A and Llandro J 2019 *Magnetic Nanoparticles in Biosensing and Medicine* (Cambridge: Cambridge University Press) p 296
[3] Buznikov N A, Safronov A P, Orue I, Golubeva E V, Lepalovskij V N, Svalov A V, Chlenova A A and Kurlyandskaya G V 2018 *Biosens. Bioelectron*. **117** 366
[4] Lukshina V A, Dmitrieva N V and Potapov A P 1996 *Phys. Met. Metallogr.* **82** (4) pp 376–378
[5] Skulkina N A, Ivanov O A, Mazeeva A K, Kuznetsov P A, Stepanova E A, Blinova O V and Mikhalitsyna E A 2018 *Phys. Met. Metallogr.* **119** (2) 127
[6] Hilzinger R and Rodewald W 2013 *Magnetic materials: fundamentals, products, properties, applications* (Hanau: Vacuumschmelze)
[7] Makhotkin V E, Shurukhin B P, Lopatin V A, Marchukov P Y and Levin Y K 1991 *Sensors and Actuators A* **27** 759
[8] Prida V M, Gorrıa P, Kurlyandskaya G V, Sanchez M L, Hernando B and Tejedor M 2003 *Nanotechnology* **14** 231
[9] Rietveld H M 1969 *J. Appl. Crystallogr*. **2** 65
[10] McHenry M E, Willard M A and Laughlin D E *Prog. Mater. Sci.* 1999 **44** 291
[11] Kurlyandskaya G V, de Cos D and Volchkov S O 2009 *J. Nondestruct. Test* (Russ.) **45** (6) 3
[12] Kurlyandskaya G V, Shcherbinin S V, Volchkov S O, Bhagat S M, Calle E, Pérez R and Vazquez M 2018 *JMMM*. **459** 154
[13] Bukreev D A, Moiseev A A, Derevyanko M S and Semirov A V 2015 *Russian Physics Journal* **58** (2) 141
[14] Nabias J; Asfour A and Yonnet J-P 2017 *IEEE Trans. Magn*. **53** 4001005
[15] Kurlyandskaya G V, Fal Miyar V, Saad A, Asua E and Rodriguez J 2007 *J. of Appl. Phys.* **101** 054505